Gastroenterology 2017;152:1449–1461

BASIC AND TRANSLATIONAL—LIVER

Metabolomic Identification of Subtypes of Nonalcoholic Steatohepatitis

Cristina Alonso,[1,*] **David Fernández-Ramos**,[2,*] Marta Varela-Rey,[2] Ibon Martínez-Arranz,[1] Nicolás Navasa,[2] Sebastiaan M. Van Liempd,[2] José L. Lavín Trueba,[2] Rebeca Mayo,[1] Concetta P. Ilisso,[2] Virginia G. de Juan,[2] Marta Iruarrizaga-Lejarreta,[1] Laura delaCruz-Villar,[2] Itziar Mincholé,[1] Aaron Robinson,[3] Javier Crespo,[4] Antonio Martín-Duce,[5] Manuel Romero-Gómez,[6] Holger Sann,[7] Julian Platon,[8] Jennifer Van Eyk,[3] Patricia Aspichueta,[9] Mazen Noureddin,[10] Juan M. Falcón-Pérez,[2] Juan Anguita,[2] Ana M. Aransay,[2] María Luz Martínez-Chantar,[2] Shelly C. Lu,[10] and José M. Mato[2]

[1]OWL Metabolomics, Parque Tecnológico de Bizkaia, Derio, Spain; [2]CIC bioGUNE, CIBERehd, Parque Tecnológico de Bizkaia, Derio, Spain; [3]Advanced Clinical Biosystems Research Institute, [10]Division of Digestive and Liver Diseases, Cedars-Sinai Medical Center, Los Angeles, California; [4]Gastroenterology and Hepatology Department, Infection, Immunity and Digestive Pathology Group, IDIVAL, Instituto de Investigación Valdecilla, Hospital Universitario Marqués de Valdecilla, Santander, Spain; [5]Faculty of Medicine and Health Science, Hospital Universitario Príncipe de Asturias, Alcalá University, Madrid, Spain; [6]Unidad de Enfermedades Digestivas, Hospital Virgen de Valme, Hospital Universitario Virgen Macarena y Virgen del Rocío, Instituto de Biomedicina de Sevilla, Universidad de Sevilla, CIBERehd, Seville, Spain; [7]Abbott Laboratories GmbH, Hannover, Germany; [8]Abbott, Allschwil, Switzerland; [9]Department of Physiology, University of the Basque Country, Biocruces Research Institute, Barakaldo, Spain

BACKGROUND & AIMS: Nonalcoholic fatty liver disease (NAFLD) is a consequence of defects in diverse metabolic pathways that involve hepatic accumulation of triglycerides. Features of these aberrations might determine whether NAFLD progresses to nonalcoholic steatohepatitis (NASH). We investigated whether the diverse defects observed in patients with NAFLD are caused by different NAFLD subtypes with specific serum metabolomic profiles, and whether these can distinguish patients with NASH from patients with simple steatosis. **METHODS:** We collected liver and serum from methionine adenosyltransferase 1a knockout (MAT1A-KO) mice, which have chronically low levels of hepatic S-adenosylmethionine (SAMe) and spontaneously develop steatohepatitis, as well as C57Bl/6 mice (controls); the metabolomes of all samples were determined. We also analyzed serum metabolomes of 535 patients with biopsy-proven NAFLD (353 with simple steatosis and 182 with NASH) and compared them with serum metabolomes of mice. MAT1A-KO mice were also given SAMe (30 mg/kg/day for 8 weeks); liver samples were collected and analyzed histologically for steatohepatitis. **RESULTS:** Livers of MAT1A-KO mice were characterized by high levels of triglycerides, diglycerides, fatty acids, ceramides, and oxidized fatty acids, as well as low levels of SAMe and downstream metabolites. There was a correlation between liver and serum metabolomes. We identified a serum metabolomic signature associated with MAT1A-KO mice that also was present in 49% of the patients; based on this signature, we identified 2 NAFLD subtypes. We identified specific panels of markers that could distinguish patients with NASH from patients with simple steatosis for each subtype of NAFLD. Administration of SAMe reduced features of steatohepatitis in MAT1A-KO mice. **CONCLUSIONS:** In an analysis of serum metabolomes of patients with NAFLD and MAT1A-KO mice with steatohepatitis, we identified 2 major subtypes of NAFLD and markers that differentiate steatosis from NASH in each subtype. These might be used to monitor disease progression and identify therapeutic targets for patients.

Keywords: Mouse Model; Lipid Metabolism; 1-Carbon Metabolism; Prognostic.

Nonalcoholic fatty liver disease (NAFLD), the leading cause of chronic liver disease in Western countries, starts with the excessive accumulation of hepatic triglycerides (TG), which in some cases progresses to nonalcoholic steatohepatitis (NASH), a condition characterized by the appearance of inflammation, cellular injury with or without fibrosis, together with steatosis.[1] Although patients with simple steatosis are thought to have a better prognosis, the overall morbidity and mortality is increased in NASH patients.[2] Hepatic steatosis arises when de novo lipogenesis and the uptake of fatty acids (FA) from circulation saturate the capacity of the liver to oxidize FA and their elimination as TG in the form of very-low-density lipoproteins (VLDLs).[1] Because there are different causes that can lead to steatosis, we hypothesized that different NAFLD subtypes may exist, reflecting the variety of mechanisms causing liver fat accumulation, and that each subtype would be characterized by

*Authors share co-first authorship.

Abbreviations used in this paper: ALT, alanine aminotransferase; DG, diglycerides; DMR, differentially methylated DNA regions; FA, fatty acids; GSH, glutathione; JC-1, 5,5,6,6-tetrachloro-1,1,3,3-tetraethylbenzimidazolyl-carbocyanineiodide; LC, liquid chromatography; MAT1A-KO, methionine adenosyltransferase 1a knockout; MS, mass spectrometry; NAFLD, nonalcoholic fatty liver disease; NASH, nonalcoholic steatohepatitis; PC, phosphatidylcholine; PCA, principal component analysis; PE, phosphatidylethanolamine; SAMe, S-adenosylmethionine; TG, triglycerides; VLDL, very-low-density lipoprotein; WT, wild-type.

Most current article

0016-5085/$36.00
http://dx.doi.org/10.1053/j.gastro.2017.01.015

EDITOR'S NOTES

BACKGROUND AND CONTEXT

Nonalcoholic fatty liver disease (NAFLD) is a consequence of defects in diverse metabolic pathways that involve hepatic accumulation of triglycerides. Features of these aberrations might determine whether NAFLD progresses to nonalcoholic steatohepatitis (NASH).

NEW FINDINGS

Our results unveiled the existence of three NAFLD metabolic phenotypes: M subtype, non-M subtype, and indeterminate subtype. All three metabolomic phenotypes were found in both simple steatosis and NASH in approximately the same proportions, which suggests that patients of the M subtype are not at higher risk to develop NASH than those with a non-M subtype. Markers that differentiate steatosis from NASH in each subtype were also identified.

LIMITATIONS

The present results showing that SAMe administration improved NASH in mice deficient in SAMe synthesis supports the concept that treatment with SAMe may benefit NAFLD patients with an M subtype. However, this point needs to be clinically proven. The non-M subtype may be a heterogeneous group in which NAFLD and its progression to NASH may result from alterations in different biochemical pathways. Comparison of other mouse models of NAFLD with the non-M subtype may clarify this point.

IMPACT

It might be used to monitor disease progression and identify therapeutic targets for patients.

a unique serum metabolomic signature. This is relevant because a better understanding of NAFLD biology will facilitate the development of personalized treatment.

We assessed this hypothesis by first analyzing the liver metabolome of methionine adenosyltransferase 1a knockout (MAT1A-KO) mice[3] to determine the mechanism causing liver fat accumulation in this model of steatohepatitis. This model is relevant to human beings because NASH patients frequently show reduced *MAT1A* mRNA levels.[4] Then, we examined if the liver metabolome is reflected in serum in mice. This is an important consideration because serum, but not liver, will be the basis for future classification of human NAFLD into subtypes. After that, we investigated whether a large cohort of NAFLD patients could be classified into different subtypes based on their similarity with the serum metabolome of MAT1A-KO mice, and searched for the existence of serum metabolic biomarkers that distinguished NASH from simple steatosis in each subtype. Finally, we assessed if S-adenosylmethionine (SAMe) administration improved steatohepatitis in MAT1A-KO mice.

Materials and Methods

Animal Experiments

Eight-month-old MAT1A-KO[5] male mice (in a C57Bl/6 background) with increases in liver enzyme levels (alanine aminotransferase [ALT] and aspartate aminotransferase) and hepatic lipid accumulation (determined by ultrasound) were given orally by gavage with vehicle (water) (n = 12) or SAMe (30 mg/kg/day, n = 12; Abbott, Chicago, IL) for 8 weeks before death. Age-matched wild-type male sibling littermates showing normal liver serum enzyme levels and ultrasound also were treated with vehicle for the same duration (n = 11). Animals were bred and housed in the CIC bioGUNE animal unit, accredited by the Association for Assessment and Accreditation of Laboratory Animal Care International. The mice were housed in groups using high-quality wood pellet hygienic litter bedding (Lignocel HBK 1500-3000; Rettenmaier & Sönne, Rosenberg, Germany) and in the presence of enrichment materials. Animals were fed with standard commercial chow animal diet (ref. 2914; Envigo, Barcelona, Spain). Submandibular and retroorbital blood samples were collected at the beginning and at the end of the experiment. Blood samples were deposited in serum-separator gel tubes (Microtainer; Becton-Dickinson, Franklin Park, NJ) and centrifuged (6000 rpm, 15 min, 4°C) for serum separation. Livers were removed and snap frozen in liquid nitrogen, optimal cutting temperature cryo-compound embedded, or formalin-fixed. All procedures were performed during the light cycle and were approved by the Diputación de Bizkaia upon a favorable assessment by the Institutional Animal Care and Use Committee at CIC bioGUNE.

Patients

Our study included a total of 535 patients who underwent liver biopsy analysis (353 with a diagnosis of simple steatosis and 182 with a diagnosis of NASH), seen at 11 participating hospitals. Among them, 377 patients were described previously by Barr et al,[6] and 158 additional patients were recruited since 2013 for this study by 3 hospitals that also participated in the first study (Hospital Universitario Marqués de Valdecilla, Hospital Universitario Príncipe de Asturias, and Hospital Virgen de Valme). Principal component analysis (PCA) of the metabolomics data showed that patients cluster together independently of the hospital of origin (Supplementary Figure 1). All patients were recruited using the following inclusion criteria: (1) age 18−75 years; (2) no known acute or chronic disease except for obesity or type 2 diabetes based on medical history, physical examination, and standard laboratory tests; and (3) alcohol consumption was less than 20 g/day for women and 30 g/day for men. Exclusion criteria included viral-, autoimmune-, hemochromatosis-, and drug-induced causes of liver disease. All of the subjects were of Caucasian origin. Additional details have been published elsewhere.[6] The institutional review board at each of the participating hospitals approved the study and written informed consent was obtained from all patients. For all subjects, blood was drawn under fasting conditions on the morning the diagnostic liver biopsy was performed. Serum was separated and stored at -80°C until analysis. Clinical data (Table 1) were collected retrospectively using patient records and laboratory values obtained at the time of biopsy.

Diagnoses were established histologically in liver biopsy specimens. The histologic diagnosis of NAFLD was established by a single liver pathologist in each participating hospital using the scoring system defined by Kleiner et al.[7] After assessment, patients were classified by the pathologists into 2 histologic groups: (1) simple steatosis (hepatic steatosis alone), and (2) NASH (presence as determined by the pathologist). None of the patients had cirrhosis.

Table 1. Clinicopathologic Characteristics of the NAFLD Patients Included in the Study

	Total			M subtype		Non-M subtype		Indeterminate	
		Simple steatosis	NASH	Simple steatosis	NASH	Simple steatosis	NASH	Simple steatosis	NASH
N (%)	535	353 (66)	182 (34)	174 (66)[a]	88 (34)[b,c]	103 (61)[d]	68 (39)	76 (75)	26 (25)
Female	69%	70%	68%	72%[a]	77%[b,c]	62%[d]	57%	77%	65%
Age, *y*	44.77 ± 11.35	44.04 ± 11.54	46.07 ± 10.94	40.31 ± 10.77[a,e]	43.64 ± 9.68[e]	48.35 ± 11.29	49.30 ± 11.44	46.77 ± 10.89	45.36 ± 11.81
BMI, kg/m^2	44.76 ± 10.78	44.50 ± 10.65	45.21 ± 11.02	48.19 ± 9.71[a,e]	49.72 ± 8.67[b,c]	40.54 ± 10.34	40.66 ± 11.18[f]	41.12 ± 10.30	42.01 ± 12.02
Fasting glucose level, *mg/dL*	113.59 ± 41.26	111.39 ± 35.86	117.31 ± 48.96	112.21 ± 35.97	119.21 ± 51.93[c]	106.32 ± 27.47	119.89 ± 50.82[f]	117.10 ± 45.01	101.05 ± 21.03
Total fasting cholesterol level, *mg/dL*	188.71 ± 41.08	187.84 ± 41.88	190.66 ± 39.45	176.88 ± 35.29[a]	175.01 ± 27.60[c]	196.59 ± 47.31	192.11 ± 43.89	191.69 ± 39.20	213.67 ± 23.56
Fasting HDL cholesterol level, *mg/dL*	47.02 ± 13.70	48.90 ± 14.26	41.83 ± 10.51	45.67 ± 10.96	42.85 ± 11.80	50.06 ± 14.77	40.66 ± 10.07	52.50 ± 17.37	48.50 ± 9.47
Fasting LDL cholesterol level, *mg/dL*	109.81 ± 33.14	109.14 ± 33.39	111.35 ± 32.87	109.17 ± 32.89	104.17 ± 23.98	107.78 ± 34.34	113.13 ± 37.22	112.29 ± 34.36	119.50 ± 19.33
Fasting triglyceride level, *mg/dL*	150.33 ± 100.19	150.57 ± 106.95	149.78 ± 83.33	124.88 ± 47.39[a]	134.38 ± 96.15	164.48 ± 92.57	156.71 ± 79.30	170.99 ± 177.11	145.62 ± 83.08
ALT level, *U/L*	39.70 ± 33.09	35.38 ± 28.39	44.62 ± 37.23	29.93 ± 20.54[a]	34.01 ± 19.45[b]	39.11 ± 32.68	55.56 ± 45.07	38.22 ± 30.97	52.76 ± 51.28

NOTE. All diagnoses were established histologically in liver biopsy specimens. Additional classification as M subtype, non-M subtype, or indeterminate was based on results detailed in the "Discovery of Two Human NAFLD Subtypes" section. Values are given as percentages or means ± SD of the mean. Results that were significantly different ($P < .05$) among the M subtype, non-M subtype, or indeterminate groups are indicated.
BMI, body mass index; HDL, high-density lipoprotein; LDL, low-density lipoprotein.
[a]Significant at $P < .05$, between M subtype and non-M subtype patients with simple steatosis.
[b]Significant at $P < .05$, between M subtype and non-M subtype patients with NASH.
[c]Significant at $P < .05$, between M subtype and indeterminate patients with NASH.
[d]Significant at $P < .05$, between non-M subtype and indeterminate patients with simple steatosis.
[e]Significant at $P < .05$, between M subtype and indeterminate patients with simple steatosis.
[f]Significant at $P < .05$, between non-M subtype and indeterminate patients with NASH.

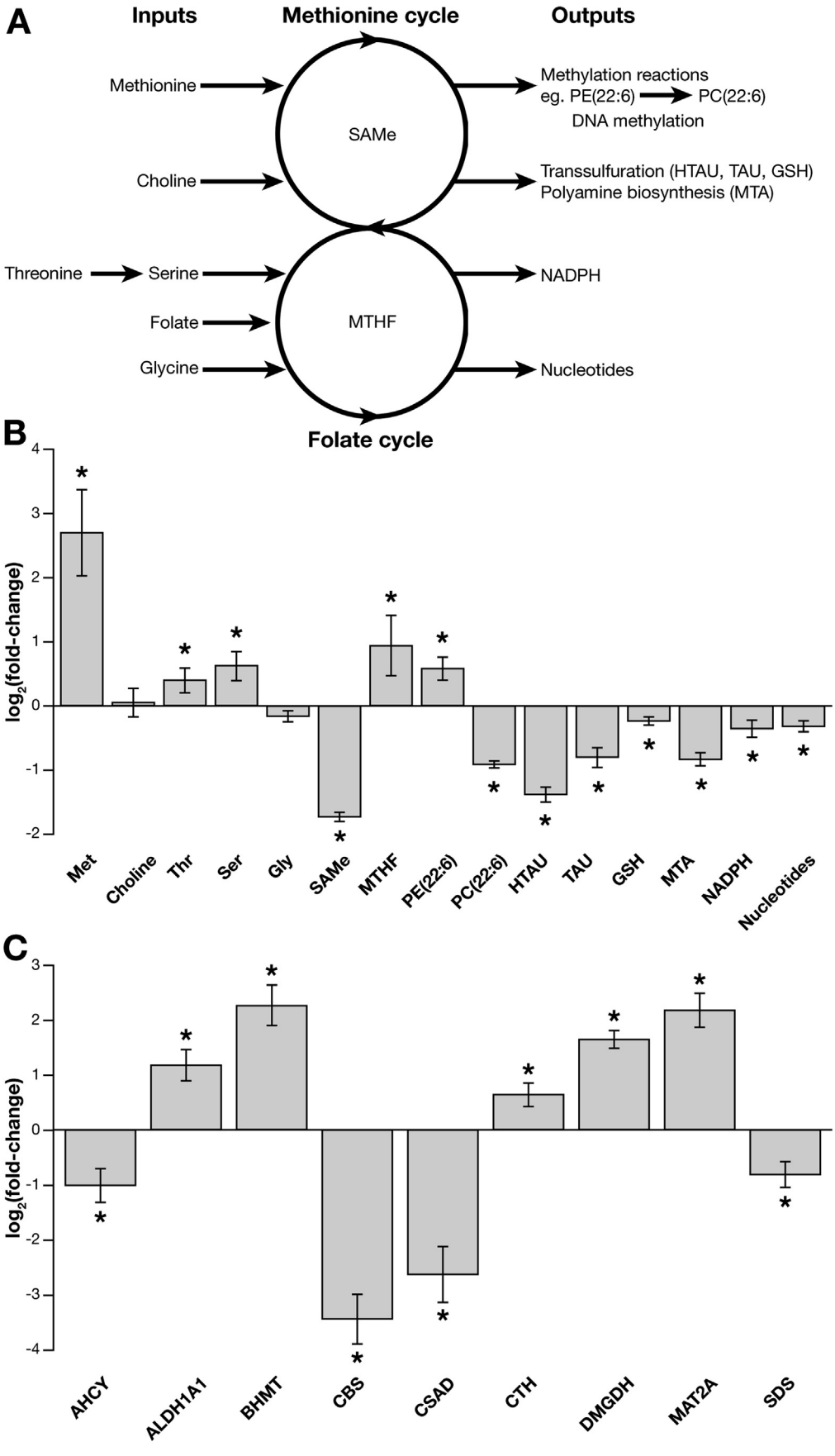
A
Inputs
Methionine cycle
Outputs
Methionine
Choline
SAMe
Methylation reactions
eg. PE(22:6) PC(22:6)
DNA methylation
Transsulfuration (HTAU, TAU, GSH)
Polyamine biosynthesis (MTA)
Threonine
Serine
Folate
Glycine
MTHF
NADPH
Nucleotides
Folate cycle
B
log2(fold-change)
Met
Choline
Thr
Ser
Gly
SAMe
MTHF
PE(22:6)
PC(22:6)
HTAU
TAU
GSH
MTA
NADPH
Nucleotides
C
log2(fold-change)
AHCY
ALDH1A1
BHMT
CBS
CSAD
CTH
DMGDH
MAT2A
SDS

Metabolomic Analysis

To determine metabolite measurements in serum, we combined a liquid chromatography (LC)–single-quadrupole mass spectrometry (MS) amino acid analysis system with 2 separate LC–time of flight–MS–based platforms that analyzed methanol/chloroform or methanol extracts for lipid analysis. For liver samples, the previous 3 LC–MS platforms were completed with a methanol/water extract analysis, covering polar metabolites. For details see the Supplementary Materials and Methods section. Absolute concentration of TG, diglycerides (DG), FA, phosphatidylethanolamines (PE), phosphatidylcholines (PC), methionine, SAMe, and methylthioadenosine was determined as described in the Supplementary Materials and Methods section.

Proteomics

For proteomics measurements, liver samples were prepared and analyzed by LC/MS/MS as described in the Supplementary Materials and Methods section. Diacylglycerol acyltransferase 2 and stearoyl–coenzyme A desaturase 1 were determined by immunoblotting.

Global DNA Methylation Profiles

Global DNA methylation was analyzed by reduced representation bisulfite sequencing, digesting DNA with *TaqI* and *MspI*, and preparing libraries with NEXTflex Bisulfite-Seq Kit (Bioo Scientific, Austin, TX) (see details in the Supplementary Materials and Methods section). Libraries were sequenced in a HiScanSQ (Illumina Inc, San Diego, CA).

Hepatocyte Mitochondrial Membrane Potential

The dye 5,5,6,6-tetrachloro-1,1,3,3-tetraethylbenzimidazolylcarbocyanineiodide (JC-1) was used to determine mitochondrial membrane potential in hepatocytes isolated from Mat1a-KO and wild-type (WT) mice as described in the Supplementary Materials and Methods section.

Histology

Histologic staining, H&E, Sudan III red, Sirius Red, and F4/80 immunostaining are described in the Supplementary Materials and Methods section.

Statistical Analysis

Data are represented as means ± SD of the mean. Differences between groups were tested using the Student t test. Significance was defined as a P value less than .05. The volcano plot analysis was performed as an effective and easy-to-interpret graph that summarizes both fold-change and t test criteria. It is a scatterplot of the negative $\log_{10}$-transformed P values from the t test against the $\log_2$ fold-change. All calculations were performed using the statistical software package R v.3.1.1 (R Development Core Team, 2011; http://cran.r-project.org). Multivariate PCA modeling was performed with the software SIMCA 14.1 (Umetrics, Malmo, Sweden).

A hierarchical clustering algorithm based on metabolite ion intensity was used to visualize the differences in metabolite signatures between samples, as well as the Ward's minimum variance method as an agglomeration method. Biochemically related compounds generally were found to cluster together. The maximum of the average of the individual silhouette widths was calculated for the clusters.[8] The cluster analysis was calculated with the cluster R package.[9] The heatmap was realized with the pheatmap R package (Kolde R. Pheatmap: Pretty Heatmaps; R package version 1.0.8; http://CRAN.R-project.org/package=pheatmap).

Results

SAMe Depletion Alters One-Carbon Metabolism

SAMe and folate metabolism are connected—they contribute to the 1-carbon metabolism that circulates 1-carbon units from different amino acids (methionine, threonine, serine, and glycine) and nutrients (choline, folate) to generate a large variety of outputs, including methylation of DNA and PE rich in polyunsaturated FA to form PC rich in polyunsaturated FA and syntheses of glutathione (GSH), polyamines, reduced nicotinamide adenine dinucleotide phosphate, and nucleotides (Figure 1*A*).[3] MAT1A deletion resulted in a reduction in hepatic SAMe, as reported in a previous study,[5] and in the content of downstream metabolites such as PC(22:6), methylthioadenosine (a biomarker of polyamine synthesis), hypotaurine, taurine, and GSH (biomarkers of the transsulfuration pathway), reduced nicotinamide adenine dinucleotide phosphate (Figure 1*B*), and DNA methylation (Supplementary Figure 2).

MAT1A deletion led also to the accumulation of methionine and upstream metabolites, such as threonine, serine, PE(22:6), and methyltetrahydrofolate in liver, and to abnormal protein content of numerous enzymes involved in 1-carbon metabolism (AHCY, ALDH1A1, BHMT, CBS, CSAD, CTH, DMGDH, MAT2A, and SDS) (Figure 1*B* and *C*).

Figure 1. SAMe depletion alters 1-carbon metabolism. (*A*) Schematic representation of 1-carbon metabolism. One-carbon metabolism circulates 1-carbon units from different inputs (methionine, choline, serine, threonine, and glycine), via SAMe and methyltetrahydrofolate (MTHF), into a large variety of outputs, such as DNA and phospholipid methylation, GSH, polyamines, reduced nicotinamide adenine dinucleotide phosphate (NADPH), and nucleotide synthesis. (*B*) Relative fold-change ($\log_2$) in the hepatic content of the main metabolites involved in 1-carbon metabolism in MAT1A-KO as compared with WT mice. MAT1A deletion induced a reduction in hepatic SAMe content and downstream metabolites, such as phosphatidylcholine with docosahexaenoic acid PC(22:6), methylthioadenosine (MTA, a biomarker of polyamine biosynthesis), GSH, hypotaurine (HTAU), and taurine (TAU) (3 key metabolites of the transsulfuration pathway), NADPH, and nucleotides. MAT1A ablation also resulted in the accumulation of methionine (Met) and upstream metabolites, such as serine (Ser), threonine (Thr), MTHF, and phosphatidylethanolamine with docosahexaenoic acid PE(22:6). (*C*) Relative fold-change ($\log_2$) in the protein content of enzymes involved in hepatic 1-carbon metabolism in MAT1A-KO as compared with WT mice. MAT1A deletion led to abnormal protein content of numerous enzymes involved in 1-carbon metabolism. AHCY, adenosylhomocysteinase; ALDH1A1, aldehyde dehydrogenase 1a1; BHMT, betaine-homocysteine S-methyltransferase; CBS, cystathionine β-synthase; CSAD, cysteine sulfinic acid decarboxylase; CTH, cystathionine γ-lyase; DMGDH, dimethylglycine dehydrogenase; MAT2A, methionine adenosyltransferase 2a; SDS, serine dehydratase. *$P < .05$.

SAMe Depletion Activates FA Uptake, Desaturation, and Esterification, Impairing FA Oxidation and VLDL Secretion

SAMe depletion was associated with hepatic accumulation of FA, DG, and TG (Figure 2*A* and *B*). Analysis of proteomics data, searching for proteins differentially expressed in MAT1A-KO that are involved in lipid metabolism, showed that the content of CD36, an FA transporter whose overexpression correlates with TG accumulation in human NAFLD,[10] was augmented significantly, as well as the protein content of stearoyl–coenzyme A desaturase 1, which is the rate-limiting enzyme in the synthesis of monounsaturated FA, the major FA of TG and membrane phospholipids (Figure 2*C*). The protein content of

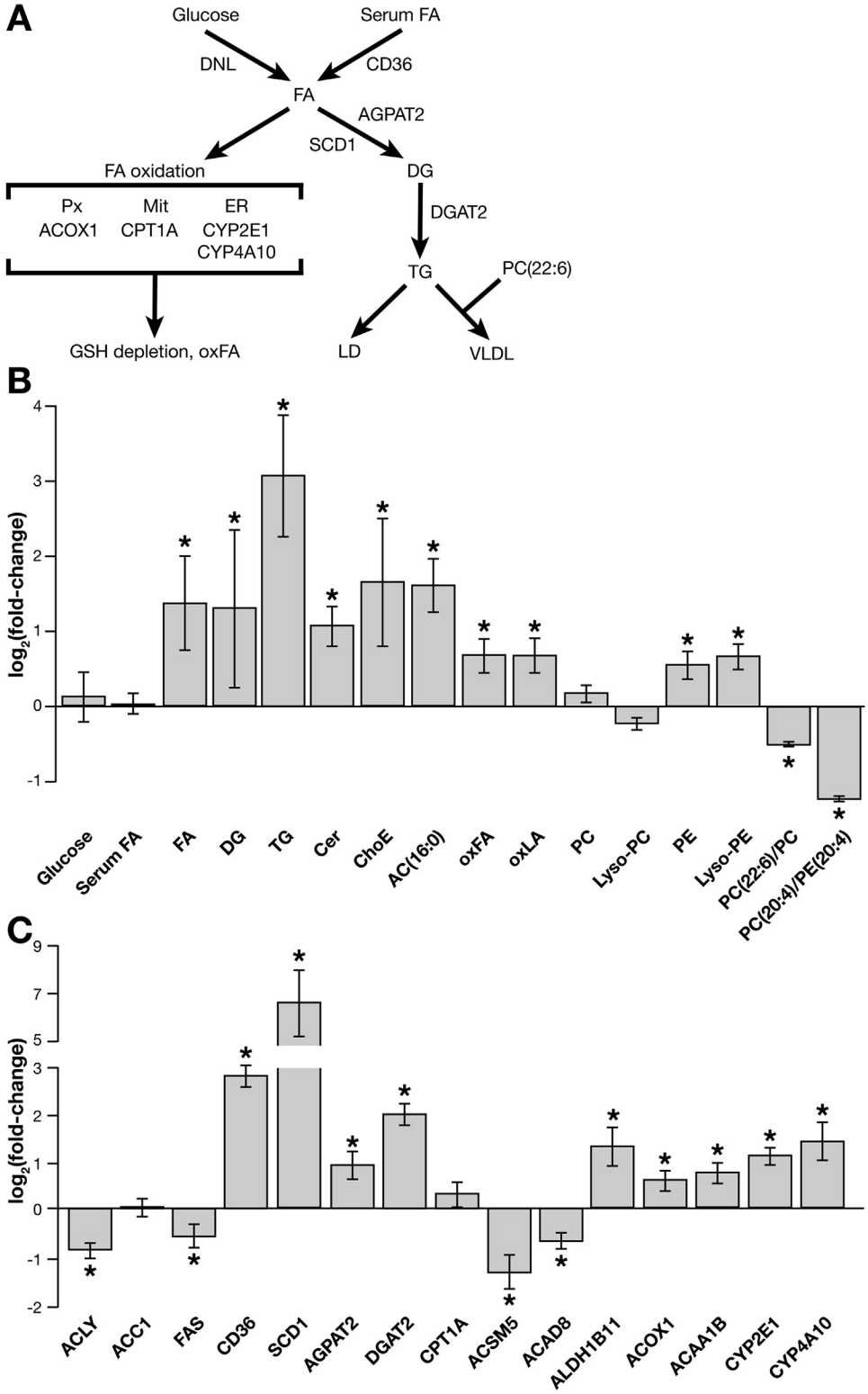

1-acylglycerol-3-phosphate O-acyltransferase 2 and diacylglycerol acyltransferase 2, 2 additional key enzymes in TG biosynthesis, also was increased in MAT1A-KO liver (Figure 2*C*). The content of the main enzymes involved in de novo lipogenesis was either normal (acetyl-CoA carboxylase 1) or reduced significantly (citrate lyase and fatty acid synthase) (Figure 2*C*). Our results also showed an accumulation of palmitoylcarnitine (AC16:0), the rate-limiting substrate in mitochondrial FA oxidation, despite having normal protein content of carnitine palmitoyltransferase 1a, which suggested an impaired oxidation of FA in MAT1A-KO mice (Figure 2*B* and *C*). Indeed, hepatocytes isolated from MAT1A-KO mice showed a loss of mitochondrial membrane polarization (Supplementary Figure 3). Notably, mitochondrial polarization was restored in MAT1A-KO hepatocytes upon incubation with SAMe (Supplementary Figure 3). Moreover, the content of oxidized FA was augmented in MAT1A-KO, which agrees with the increased protein content of aldehyde dehydrogenase 1 family member B1, a critical mitochondrial enzyme involved in lipid peroxidation (Figure 2*B* and *C*). Accordingly, MAT1A-KO livers showed decreased content of several enzymes that catalyze the mitochondrial oxidation of FA (acyl-CoA synthetase medium chain family member 5 and acyl-CoA dehydrogenase family member 8), and augmented the content of key enzymes involved in peroxisomal (acyl-CoA oxidase 1 and acyl-CoA acetyltransferase) and endoplasmic reticulum (cytochrome P450 enzyme 2E1 and cytochrome P450 enzyme A10) FA oxidation (Figure 2*C*). Finally, SAMe depletion caused a reduction in the ratio of PC(22:6)/PC and PC(20:4)/PE(20:4), both of which are indicators of reduced phosphatidylethanolamine N-methyltransferase activity (Figure 2*B*). Phosphatidylethanolamine N-methyltransferase activity is needed for VLDL assembly and export, and its deletion makes mice more prone to develop fatty liver.[11] Notably, MAT1A-KO mice have reduced VLDL secretion.[12] Collectively, the aforementioned results indicate that the increased flow of peripheral fat stored in the adipose tissue to the liver by way of the serum FA pool, together with an impaired export of TGs into VLDL and decreased oxidation of FA in the mitochondria, is the main source of lipids contributing to fatty liver in MAT1A-KO mice.

These findings prompted us to speculate that excess FA may be rerouted toward other pathways, such as ceramide synthesis. Consistent with this hypothesis, livers from MAT1A-KO mice showed an accumulation of ceramides (Figure 2*B*). Moreover, MAT1A-KO mice showed high levels of cholesteryl esters, PE and Lyso-PE, which agrees with the work of others showing the importance of Lyso-phospholipids in human NASH,[13,14] and a decrease in the PC/PE ratio (Figure 2*B* and *C*), which would indicate that a deficiency in liver SAMe has far-reaching effects on lipid metabolism.

Discovery of Two Human NAFLD Subtypes

To investigate if NAFLD patients show alterations in hepatic metabolism similar to those observed in MAT1A-KO mice, we first analyzed if the serum metabolomic profile of MAT1A-KO mice reflected the liver metabolomic profile. Accordingly, we compared the liver metabolomic profile of MAT1A-KO and WT mice and generated a list with the fold-change and *P* values for each metabolite (Supplementary Table 1). Then we proceeded similarly for the serum metabolomic profiles of MAT1A-KO and WT mice and generated a second list showing the fold-change and *P* values for each metabolite (Supplementary Table 1). Finally, we analyzed if the serum metabolomic profile reflected hepatic metabolism by comparing the common metabolites in both sets of data. As shown in Figure 3, there is a statistically significant correlation ($R^2 = 0.45$; $P < 1E\text{-}04$) between both metabolomic profiles.

Subsequently, we selected the top 50 serum metabolites that differentiated more significantly between MAT1A-KO and WT mice (Figure 4*A*). Silhouette cluster analysis[8] showed that this signature subclassified a cohort of 535 patients with biopsy-proven NAFLD (353 diagnosed with simple steatosis and 182 diagnosed with NASH) into 2 main clusters, a first cluster showing a serum metabolic profile similar to that observed in the MAT1A-KO mice (M-subtype)

Figure 2. SAMe depletion activates FA uptake and esterification, whereas FA oxidation and VLDL secretion are impaired. (*A*) Schematic representation of hepatic lipid metabolism. Hepatic FAs originate from serum and through de novo lipogenesis (DNL). FA can be either oxidized in the mitochondria (Mit) or esterified to form TGs, which are stored in lipid droplets (LD), used to form other lipids, such as phospholipids, ceramides (Cer), and cholesteryl esters (ChoE) (not shown), or exported into blood as VLDLs. The formation of VLDL particles requires PC molecules rich in polyunsaturated FA, such as PC(22:6). The rate-limiting step in mitochondrial β-oxidation is carnitine palmitoyltransferase 1a (CPT1A), which forms palmitoylcarnitine (AC16:0). The accumulation of FA in the cytoplasm increases their oxidation in peroxisomes (Px) and endoplasmic reticulum (ER). The first step in Px β-oxidation is acyl-CoA oxidase 1 (ACOX1), which generates reactive oxygen species. ER ω-oxidation, which is catalyzed by cytochrome P450 (CYP) enzymes, such as CYP2E1 and CYP4A10, also generates reactive oxygen species. In its turn, ROS induces GSH depletion and produces oxidized FA (oxFA), such as linoleic acid–derived oxidized FA (oxLA), which can lead to fibrosis and cell death. (*B*) Relative fold-change (log_2) in the hepatic content of the main metabolites involved in lipid metabolism in MAT1A-KO as compared with WT mice. AC(16:0), palmitoylcarnitine; oxFA, oxidized FA; oxLA, linoleic acid (18:2)-derived oxidized FA; lyso-PC, lyso-phosphatidylcholine; lyso-PE, lyso-phosphatidylethanolamine; PC(22:6)/PC, ratio PC with docosahexaenoic acid/total PC; PC(20:4)/PE(20:4) and ratio PC/PE with arachidonic acid. (*C*) Relative fold-change (log_2) in the content of proteins involved in liver lipid metabolism in MAT1A-KO as compared with WT mice. DNL enzymes: ACLY, citrate lyase; ACC1, acetyl-CoA carboxylase 1; FAS, fatty acid synthase. FA transport: CD36, fatty acid translocase. FA esterification: SCD1, stearoyl-CoA desaturase 1; AGPAT2, 1-acylglycerol-3-phosphate O-acyltransferase 2; and DGAT2, diacylglycerol acyltransferase 2. Mitochondrial FA β-oxidation: CPT1A, carnitine palmitoyltransferase 1a; ACSM5, acyl-CoA synthetase medium chain family member 5; ACAD8, acyl-CoA dehydrogenase family member 8; ALDH1B1, aldehyde dehydrogenase 1 family member B1. Peroxisomal FA β-oxidation: ACOX1, acyl-CoA oxidase 1; ACAA1B, acyl-CoA acetyltransferase. Endoplasmic reticulum FA ω-oxidation: CYP2E1 and CYP4A10. $^*P < .05$.

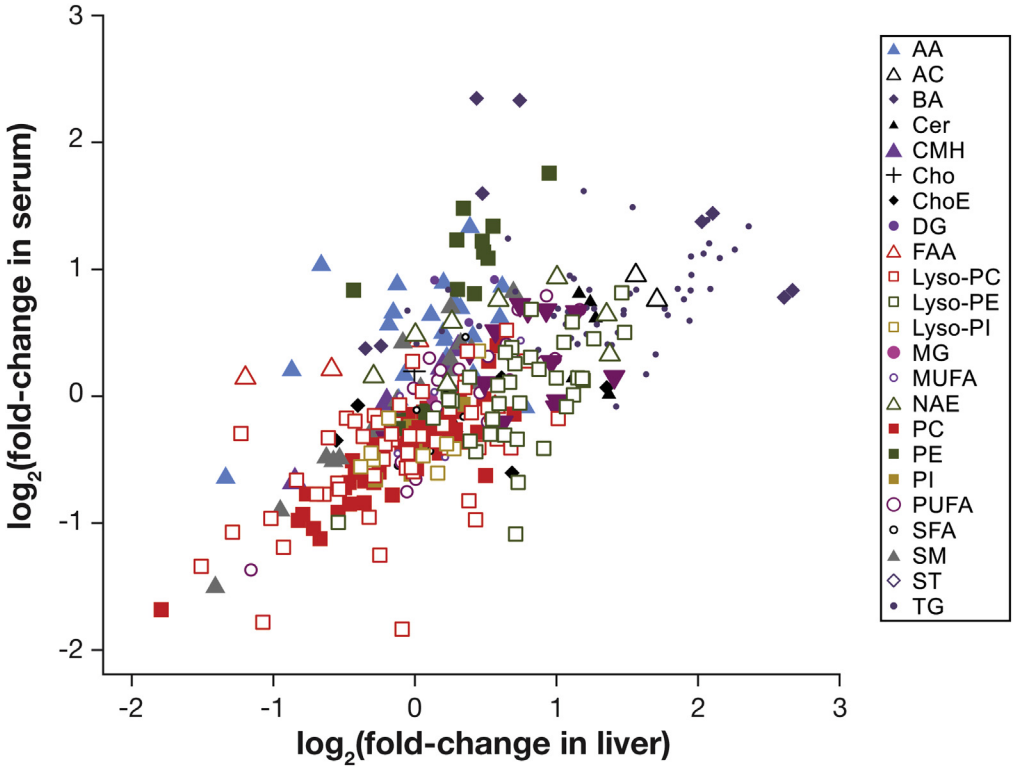

Figure 3. The serum metabolomic profile reflects hepatic metabolism. Comparison of liver and serum metabolomics profiles of MAT1A-KO mice. Each *point* represents the $\log_2$(fold-change) of individual metabolic ion features of MAT1A-KO compared with WT mice in serum and liver. A list with the $\log_2$(fold-change) and *P* value for each individual metabolite in serum and liver is given in Supplementary Table 1. $R^2 = 0.45$; $P = 1E\text{-}04$. AA, amino acid; AC, acyl carnitine; BA, bile acid; Cer, ceramide; CMH, monohexosylceramide; Cho, cholesterol; ChoE, cholesteryl ester; FAA, fatty acyl amide; Lyso-PC, lyso- phosphatidylcholine; Lyso-PE, lyso-phosphatidylethanolamine; Lyso-PI, lyso-phosphatidylinositol; MG, monoglyceride; MUFA, monounsaturated fatty acid; NAE, N-acylethanolamines; PI, phosphatidylinositol; PUFA, polyunsaturated fatty acid; SFA, saturated fatty acid; SM, sphingomyelin; ST, steroid.

and a second cluster showing a different profile (non–M-subtype) (Figure 4*B*). For validation, we followed the procedure described in Figure 5. First, samples were partitioned randomly (50/50) into 2 cohorts (estimation and validation) with equal proportional representation of steatosis/NASH and males/females. Then, clustering analysis based on the selected top 50 MAT1A-KO biomarkers generated 2 main clusters and patients were classified into M and non-M subtypes. Based on the complete metabolic profile (N = 328 metabolites) of the human serum samples, biomarkers that differentiated between NASH and steatosis significantly were selected and validated by comparison between the results in estimation and validation cohorts. After 1000-fold repetition of this random partition, each time with equal proportional representation of steatosis/NASH and males/females, the frequency distribution of the metabolites that differentiated significantly between NASH and steatosis in the M and non-M subtypes was determined, and those showing a reproducibility of at least 700 times in 1000 repetitions were selected. A ranked NASH biomarkers list per subtype, showing the reproducibility and *P* value, was generated (Supplementary Table 2). The M subtype NASH biomarker list contained 54 metabolites: 5 amino acids, 8 fatty acyls (6 FA and 2 oxidized FA), 3 TGs, 37 phospholipids (4 PC, 15 Lyso-PC, 7 PE, 10 Lyso-PE, and 1 phosphatidylinositol), and 1 sphingomyelin (Figure 5 and Supplementary Table 2A). Twenty-nine of these metabolites had a reproducibility of ≥90%. Interestingly, 25 of the 54 biomarkers were lyso-phospholipids. The non-M subtype NASH biomarkers list consisted of 6 metabolites: 1 amino acid, 1 FA, 1 bile acid, and 3 TGs (Figure 5 and Supplementary Table 2B).

The frequency distribution of the NAFLD patients into the M and non-M subtypes also was calculated (Figure 5). Following the criteria based on ≥70% reproducibility, 262 patients (49%) were classified as M subtype and 171 (32%) were classified as non-M subtype. The remaining 102 patients (19%) showed a reproducibility of less than 70% and could not be classified as either M or non-M subtype (indeterminate group). Supplementary Table 3 summarizes the serum metabolites associated with the MAT1A-KO serum metabolomics profile in the human subtypes.

Although there was a significant excess of females in the M subtype steatosis and NASH groups compared with the non-M subtype (Table 1), PCA of serum metabolome showed no differences between females and males (Supplementary Figure 4). In this study, female mice were not tested. The body mass index in the M group was significantly higher, whereas the age and ALT level were lower than in the non-M subtype in both simple steatosis

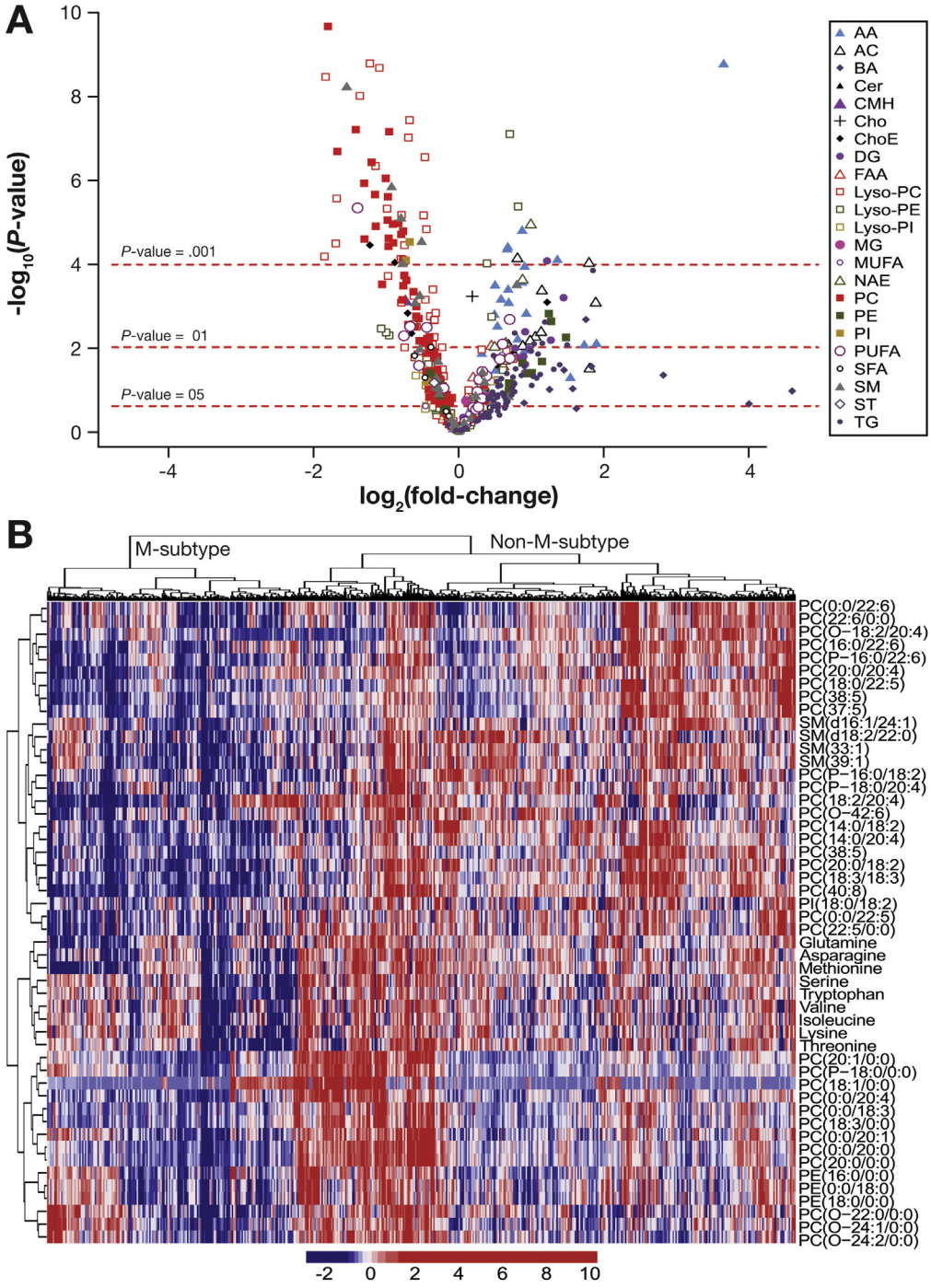

Figure 4. Identification of a subset of NAFLD patients showing a MAT1A-KO serum metabolomic profile. (*A*) Volcano plot representation indicating the -$\log_{10}$(*P* value) and $\log_2$(fold-change) of individual serum metabolic ion features of MAT1A-KO compared with WT mice. AA, amino acid; AC, acyl carnitine; BA, bile acid; Cer, ceramide; CMH, monohexosylceramide; Cho, cholesterol; ChoE, cholesteryl ester; FAA, fatty acyl amide; Lyso-PC, lyso-phosphatidylcholine; Lyso-PE, lyso-phosphatidylethanolamine; Lyso-PI, lyso-phosphatidylinositol; MG, monoglyceride; MUFA, monounsaturated fatty acid; NAE, N-acylethanolamine; PI, phosphatidylinositol; PUFA, polyunsaturated fatty acid; SFA, saturated fatty acid; SM, sphingomyelin; ST, steroid. (*B*) Heatmap representation of the serum metabolomic profile from 535 patients with biopsy-confirmed NAFLD. Each data *point* corresponds to the relative ion abundance of a given metabolite (*vertical axis*) in an individual patient's serum. Metabolite selection is based on the top 50 serum metabolites that differentiated more significantly between MAT1A-KO and WT mice. The hierarchical clustering is based on the optimum average silhouette width, dividing the classification of the samples into 2 groups: the first cluster resembles the serum metabolomic profile observed in the MAT1A-KO mice (M subtype), and the second cluster shows a different metabolomic profile (non-M subtype).

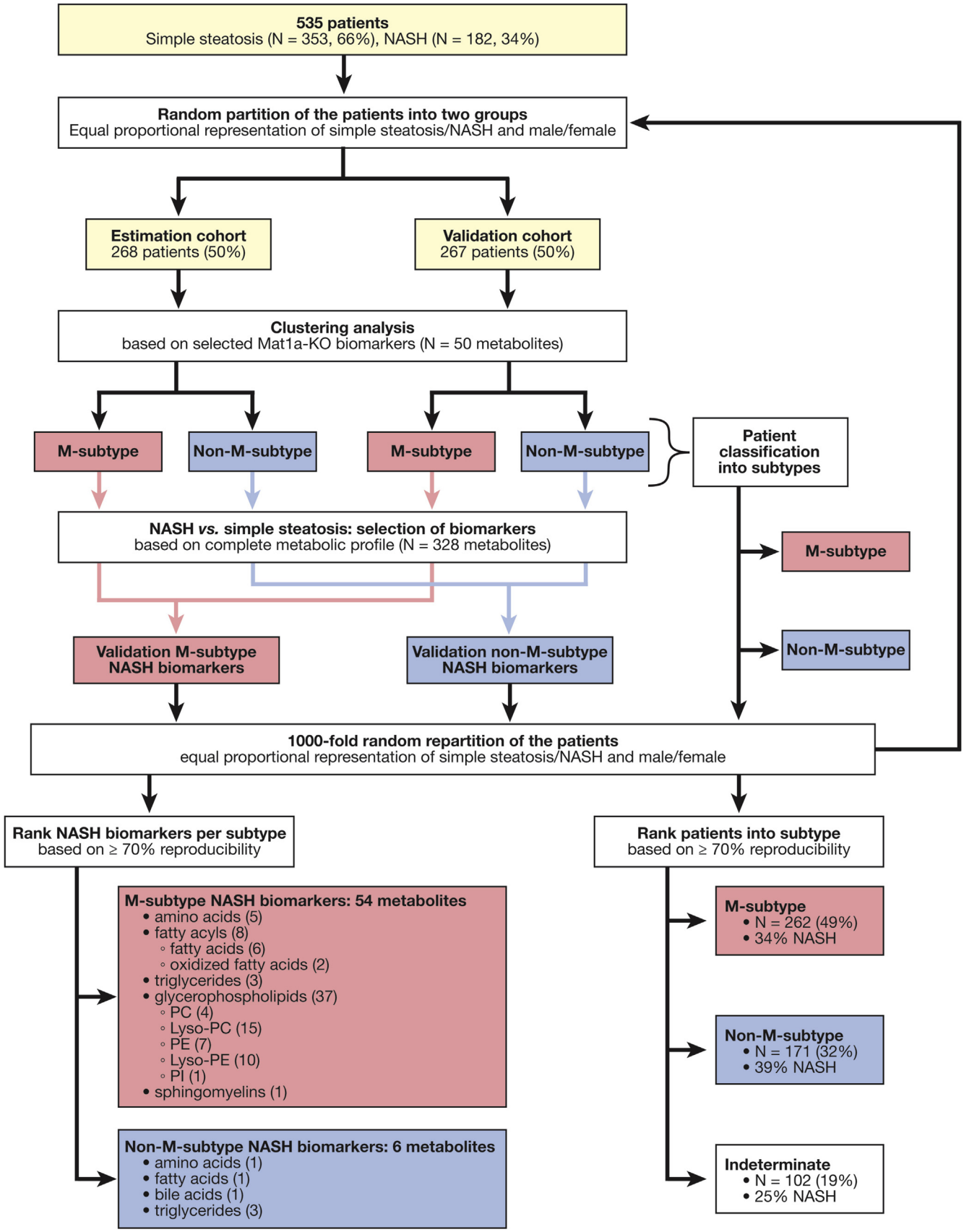
535 patients
Simple steatosis (N = 353, 66%), NASH (N = 182, 34%)
Random partition of the patients into two groups
Equal proportional representation of simple steatosis/NASH and male/female
Estimation cohort
268 patients (50%)
Validation cohort
267 patients (50%)
Clustering analysis
based on selected Mat1a-KO biomarkers (N = 50 metabolites)
M-subtype
Non-M-subtype
M-subtype
Non-M-subtype
Patient classification into subtypes
NASH vs. simple steatosis: selection of biomarkers
based on complete metabolic profile (N = 328 metabolites)
M-subtype
Non-M-subtype
Validation M-subtype NASH biomarkers
Validation non-M-subtype NASH biomarkers
1000-fold random repartition of the patients
equal proportional representation of simple steatosis/NASH and male/female
Rank NASH biomarkers per subtype
based on ≥ 70% reproducibility
Rank patients into subtype
based on ≥ 70% reproducibility
M-subtype NASH biomarkers: 54 metabolites
• amino acids (5)
• fatty acyls (8)
◦ fatty acids (6)
◦ oxidized fatty acids (2)
• triglycerides (3)
• glycerophospholipids (37)
◦ PC (4)
◦ Lyso-PC (15)
◦ PE (7)
◦ Lyso-PE (10)
◦ PI (1)
• sphingomyelins (1)
Non-M-subtype NASH biomarkers: 6 metabolites
• amino acids (1)
• fatty acids (1)
• bile acids (1)
• triglycerides (3)
M-subtype
• N = 262 (49%)
• 34% NASH
Non-M-subtype
• N = 171 (32%)
• 39% NASH
Indeterminate
• N = 102 (19%)
• 25% NASH

and NASH (Table 1). Among the M-subtype group, the percentage of NASH patients (34%) was the same as that in the total cohort of NAFLD patients (34%), and slightly, but significantly, lower than that observed in patients classified as non-M subtype (39%) and higher than in the indeterminate group of patients (25%) (Table 1).

Administration of SAMe Improves Steatohepatitis

The bioavailability of orally administered SAMe is poor because of a significant first-pass effect and rapid hepatic metabolism.[15] The SAMe half-life is approximately 5 minutes.[16] Consistent with this, we previously observed that after SAMe intraperitoneal injection, liver SAMe content increased rapidly, reaching a peak in 15 minutes and recovering basal levels 4 hours after injection.[17] Here, we found that the concentration of serum and liver SAMe in MAT1A-KO mice that received SAMe was not significantly different from KO mice that received the vehicle (not shown), which agrees with the short half-life of SAMe because mice were killed 24 hours after the last administration of SAMe. Analysis of the differentially methylated DNA regions (DMRs) in SAMe-given MAT1A-KO mice compared with vehicle-given MAT1A-KO animals showed that SAMe administration increased DNA methylation (Supplementary Figure 2), which confirms the intracellular utilization of orally administered SAMe. DMRs identified in MAT1A-KO mice that received SAMe were distributed across all chromosomes and the majority of these regions were hypomethylated in mutant mice that received the vehicle. The relevance of these findings was confirmed by the observation that human NASH associates with hypomethylation of liver DNA.[18]

Finally, we found that SAMe administration improved liver function, as indicated by a reduction in serum transaminase levels and liver histology (Figure 6). Mice that received SAMe showed a reduction of lipid accumulation, as quantified by morphometry of Sudan red–stained area (11-fold as compared with MAT1A-KO mice that received vehicle; $P = 2.0E-04$) (Figure 6*A*). Mice given SAMe also showed decreased liver fibrosis, as quantified by morphometry of Sirius red staining (3-fold as compared with MAT1A-KO mice given the vehicle; $P = 2.6E-02$) (Figure 6*A*). Furthermore, livers from MAT1A-KO mice given SAMe showed a reduction of inflammation as quantified by morphometry of F4/80 (3-fold as compared with MAT1A-KO mice given the vehicle; $P = 3.0E-03$) (Figure 6*A*).

Discussion

Our results provide evidence that MAT1A protein functions as an integrator of the cellular metabolic status and that its deletion not only affects hepatic metabolism downstream of SAMe (DNA and phospholipid methylation, polyamine, and GSH synthesis), but also leads to an imbalance in the circulation of 1-carbon units from specific amino acids (methionine, threonine, serine, and glycine) to folates, altering an unparalleled diversity of cellular processes ranging from the biosynthesis of lipids, proteins, and amino acids, to the regulation of mitochondrial polarization and function. Genetic and functional evidence support the importance of the activity of the serine-glycine-folate-methionine pathway in tumorigenesis.[19] We propose that these changes, although many are likely to be part of a compensatory response, will create a metabolic environment that favors steatohepatitis development and, perhaps, its progression to hepatocellular carcinoma in MAT1A-KO mice.[20] Our results show that SAMe depletion induced hypomethylation of DNA regions in MAT1A-KO as compared with WT mice. In human NAFLD, hepatic DNA hypomethylation has been found to be associated with more advanced NAFLD.[18] Although much remains to be learned in this area, this is probably an important driver of NASH in MAT1A-KO mice because SAMe administration significantly decreased the number of DMRs and improved liver function and histology.

Our results unveiled the existence of 3 NAFLD metabolic phenotypes: M subtype, non-M subtype, and indeterminate subtype. All 3 metabolomic phenotypes were found in both simple steatosis and NASH in approximately the same proportions, which suggests that patients of the M subtype are not at higher risk to develop NASH than those with a non-M subtype. Whether the natural course of the different subtypes differ cannot be addressed. This, however, does not preclude the diagnostic value of identifying patients of the M subtype because approximately 50% of all NAFLD patients show this phenotype and those patients are likely to benefit from SAMe or other specific treatments to be developed in the future. The M phenotype occurred significantly more frequently in females as compared with the non-M subtype. The body mass index in the M subtype also was significantly

Figure 5. Scheme for the identification and validation of NAFLD subtypes and NASH biomarkers. Serum samples from 535 patients with biopsy-proven NAFLD (353 simple steatosis and 182 NASH) were partitioned randomly (50/50) into 2 cohorts (estimation and validation cohorts) with an equal proportion of steatosis/NASH and males/females. Clustering analysis, based on the 50 serum metabolites that differentiated more significantly between MAT1A-KO and WT mice (see Figure 4), generated 2 main clusters and patients were classified into M and non-M subtypes. Based on the complete metabolic profile (N = 328 metabolites) of the human serum samples, biomarkers that differentiated significantly between NASH and simple steatosis were selected and validated by comparison between the results in estimation and validation cohorts. After 1000-fold repetition of this random partition, each time with equal proportional representation of simple steatosis/NASH and males/females, the frequency distribution of the metabolites that differentiated significantly between NASH and simple steatosis in the M and non-M subtypes was determined, and those showing a reproducibility of at least 700 times in 1000 repetitions were selected. The frequency distribution of the NAFLD patients into the M and non-M subtypes also was calculated. Following the criteria based on ≥70% reproducibility, 262 patients (49%) were classified as M subtype and 171 (32%) were classified as non-M subtype. The remaining 102 patients (19%) showed a reproducibility of less than 70% and could not be classified as either M or non-M subtype (indeterminate group). Lyso-PC, lyso- phosphatidylcholine; Lyso-PE, lyso- phosphatidylethanolamine; PI, phosphatidylinositol.

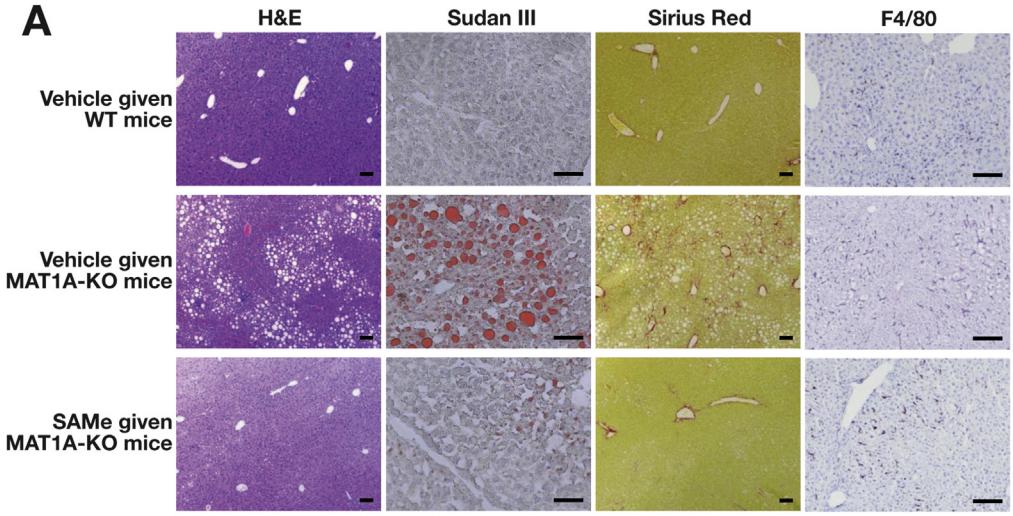

	Sudan III (a.u. ± SD)	Sirius Red (a.u. ± SD)	F4/80 (a.u. ± SD)
WT + vehicle	1.149 ± 1.06*	1.359 ± 0.83*	0.693 ± 0.86
MAT1A-KO + vehicle	21.502 ± 14.72	3.411 ± 2.81	1.291 ± 0.90
MAT1A-KO + SAMe	2.01 ± 2.98*	1.329 ± 0.73*	0.4 ± 0.31*

*$P < .05$

B

	ALT (UL ± SD)	AST (UL ± SD)	Cholesterol (mg/dl ± SD)	Triglycerides (mg/dl ± SD)
WT + vehicle (before)	31.3 ± 5.0	88.3 ± 20.9	146.7 ± 16.8	136.3 ± 26.6
WT + vehicle (after)	20.1 ± 10.5*	43.2 ± 16.2*	110.2 ± 24.7*	105.3 ± 25.1
MAT1A-KO + vehicle (before)	103.3 ± 48.9	71.8 ± 20.2	99.8 ± 21.8	149.5 ± 41.3
MAT1A-KO + vehicle (after)	137.2 ± 104.8	107.0 ± 46.1*	106.8 ± 27.0	121.5 ± 38.1*
MAT1A-KO + SAMe (before)	220.1 ± 255.4	128.3 ± 94.3	105.7 ± 28.7	170.0 ± 54.6
MAT1A-KO + SAMe (after)	40.5 ± 22.9*	63.7 ± 34.9*	93.9 ± 36.7	114.1 ± 41.5*

*$P < .05$

Figure 6. Effect of SAMe administration on histology and serology in MAT1A-KO mice. (*A*) Representative images of H&E, Sudan III red, Sirius red, and F4/80 immunofluorescence staining of liver tissues after 8 weeks of SAMe (30 mg/kg/day) or vehicle administration are shown. Sizing bars correspond to 100 μm for H&E and Sirius Red, and 50 μm for Sudan III and F4/80. Quantitative analyses are shown in the *table*. Results that were significantly different ($P < .05$) from vehicle-given MAT1A-KO mice are indicated. Data shown represent the mean of 12 vehicle-given MAT1A-KO, 12 SAMe-given MAT1A-KO, and 11 vehicle-given WT animals. (*B*) Effect of SAMe administration on serum parameters. For each group of animals (WT + vehicle, MAT1A-KO + vehicle, and MAT1A-KO + SAMe), results that were significantly different ($P < .05$) before and after administration are indicated. Twelve SAMe-treated MAT1A-KO, 12 vehicle-given MAT1A-KO, and 11 vehicle-given WT mice were analyzed.

higher, whereas the age and ALT level were significantly lower than in the non-M subtype. We obtained a second metabolic signature that could separate NAFLD patients of the M subtype into NASH and simple steatosis. This signature included methionine, several PE, Lyso-PE, PC, and Lyso-PC. Because these metabolites are biomarkers of impaired 1-carbon metabolism, these results support the concept that altered SAMe level is a determinant that switches from benign steatosis to NASH. This agrees with the finding that NASH patients with more advanced disease often show decreased *MAT1A* expression.[4]

The finding that the serum metabolomic profile of MAT1A-KO mice reflects the liver metabolomics profile supports the hypothesis that patients with an M metabolic phenotype have lower MAT1A activity. Because the M metabolic phenotype was found in both simple steatosis and NASH, this would suggest that impaired SAMe synthesis occurs early in the development of NAFLD in this subgroup of patients. Human liver MAT1A protein levels show a Gaussian frequency distribution with a large variation between individuals.[21] Whether individuals with lower MAT1A protein levels have lower hepatic SAMe content and are at higher risk to develop NAFLD needs to be determined. Variations in hepatic MAT1A protein among individuals do not correlate with age or any common *MAT1A* genetic polymorphism,[21] and there is evidence indicating that *MAT1A* expression is not regulated by the circadian rhythm.[22] Whether microRNAs, which have been found to regulate *MAT1A* expression,[23] are involved in determining MAT1A protein content is not known. Alternatively, the situation may be more complicated and may be that the M subtype was related to alterations in MAT1A enzymatic activity and other enzyme heterogeneities.

Because there is considerable interest in the use of SAMe to treat NASH,[24] these findings suggest that NASH patients

showing an M subtype serum metabolomic profile may be best suited to benefit from SAMe treatment. The present results showing that SAMe treatment improved NASH in mice deficient in SAMe synthesis supports this concept. The non-M subtype may be a heterogeneous group in which NAFLD and its progression to NASH may result from alterations in different biochemical pathways. Comparison of other mouse models of NAFLD with the non-M subtype may clarify this point.

Supplementary Material

Note: To access the supplementary material accompanying this article, visit the online version of *Gastroenterology* at www.gastrojournal.org, and at http://dx.doi.org/10.1053/j.gastro.2017.01.015.

References

1. Cohen JC, Horton JD, Hobbs HH. Human fatty liver disease: old questions and new insights. Science 2011; 332:1519–1523.
2. Angulo P. Long-term mortality in nonalcoholic fatty liver disease: is liver histology of any prognostic significance? Hepatology 2010;51:373–375.
3. Lu SC, Mato JM. S-adenosylmethionine in liver health, injury, and cancer. Physiol Rev 2012;92:1515–1542.
4. Moylan CA, Pang H, Dellinger A, et al. Hepatic gene expression profiles differentiate presymptomatic patients with mild versus severe nonalcoholic fatty liver disease. Hepatology 2014;59:471–482.
5. Lu SC, Alvarez L, Huang ZZ, et al. Methionine adenosyltransferase 1A knockout mice are predisposed to liver injury and exhibit increased expression of genes involved in proliferation. Proc Natl Acad Sci U S A 2001;98:5560–5565.
6. Barr J, Caballeria J, Martínez-Arranz I, et al. Obesity-dependent metabolic signatures associated with nonalcoholic fatty liver disease progression. J Proteome Res 2012;11:2521–2532.
7. Kleiner DE, Brunt EM, Van Natta M, et al. Design and validation of a histological scoring system for nonalcoholic fatty liver disease. Hepatology 2005;41:1313–1321.
8. Rousseeuw PJ. Silhouettes: a graphical aid to the interpretation and validation of cluster analysis. J Comput Appl Math 1987;20:53–65.
9. Maechler M, Rousseuw PJ, Struyf A, et al. Cluster: cluster analysis basics and extensions. R package version 2.0.4. Available at https://www.r-project.org/.
10. **Greco D, Kotronen A**, Westerbacka J, et al. Gene expression in human NAFLD. Am J Physiol Gastrointest Liver Physiol 2008;294:G1281–G1287.
11. Vance DE. Physiological roles of phosphatidylethanolamine N-methyltransferase. Biochim Biophys Acta 2013; 1831:626–632.
12. Cano A, Buque X, Martinez-Una M, et al. Methionine adenosyltransferase 1A gene deletion disrupts hepatic very low-density lipoprotein assembly in mice. Hepatology 2011;54:1975–1986.
13. **Han MS, Park SY**, Shinzawa K, et al. Lysophosphatidylcholine as a death effector in the lipoapoptosis of hepatocytes. J Lipid Res 2008;49:84–97.
14. Kakisaka K, Cazanave SC, Fingas CD, et al. Mechanisms of lysophosphatidylcholine-induced hepatocyte lipoapoptosis. Am J Physiol Gastrointest Liver Physiol 2012;302:G77–G84.
15. Loehrer FM, Schwab R, Angst CP, et al. Influence of oral S-adenosylmethionine on plasma 5-methyltetrahydrofolate, S-adenosylhomocysteine, homocysteine and methionine in healthy humans. J Pharmacol Exp Ther 1997;282: 845–850.
16. Mudd SH, Poole JR. Labile methyl balances for normal humans on various dietary regimens. Metabolism 1975; 24:721–735.
17. Lu SC, Ramani K, Ou X, et al. S-adenosylmethionine in the chemoprevention and treatment of hepatocellular carcinoma in a rat model. Hepatology 2009;50:462–471.
18. Murphy SK, Yang H, Moylan CA, et al. Relationship between methylome and transcriptome in patients with nonalcoholic fatty liver disease. Gastroenterology 2013; 145:1076–1087.
19. Locasale JW. Serine, glycine and one-carbon units: cancer metabolism in full circle. Nat Rev Cancer 2013; 13:572–583.
20. **Martinez-Chantar ML, Corrales FJ**, Martinez-Cruz LA, et al. Spontaneous oxidative stress and liver tumors in mice lacking methionine adenosyltransferase 1A. FASEB J 2002;16:1292–1294.
21. Ji Y, Nordgren KK, Chai Y, et al. Human liver methionine cycle: MAT1A and GNMT gene resequencing, functional genomics, and hepatic genotype-phenotype correlation. Drug Metab Dispos 2012;40:1984–1992.
22. Kim J-S, Coon SL, Blackshaw S, et al. Methionine adenosyltransferase:adrenergic-cAMP mechanism regulates a daily rhythm in pineal expression. J Biol Chem 2005;280:677–684.
23. Yang H, Cho ME, Li TW, et al. MicroRNAs regulate methionine adenosyltransferase 1A expression in hepatocellular carcinoma. J Clin Invest 2013;123:285–298.
24. Anstee QM, Day CP. S-adenosylmethionine (SAMe) therapy in liver disease: a review of current evidence and clinical utility. J Hepatol 2012;57:1097–1109.

Author names in bold designate shared co-first authorship.

Received March 2, 2016. Accepted January 9, 2017.

Reprint requests
Address requests for reprints to: José M. Mato, PhD, CIC bioGUNE, Parque Tecnológico de Bizkaia, 48160 Derio, Spain. e-mail: jmmato@cicbiogune.es; fax: +34 94 406 1 01.

Conflicts of interest
These authors disclose the following: José M. Mato is a consultant and/or speaker for Abbott, Galmed, and OWL Metabolomics; Mazen Noureddin is a consultant for Abbott and has been on the scientific advisory board or a speaker for OWL and Echosens; Holger Sann and Julian Platon are employees of Abbott; and Cristina Alonso, Ibon Martínez-Arranz, Rebeca Mayo, Marta Iruarrizaga-Lejarreta, and Itziar Mincholé are employees of OWL Metabolomics. The remaining authors disclose no conflicts.

Funding
This work was supported by National Institutes of Health grant R01AT001576 (S.C.L. and J.M.M.), Plan Nacional of I+D SAF 2014-52097R (J.M.M.) and SAF 2014-54658R (M.L.M.-C.), MINECO-ISCiii PIE14/00031 (M.L.M.-C. and J.M.M.), CIBERehd-ISCiii (J.M.M., M.L.M.-C., and A.M.A.), and Basque Government Health Department 2013111114 and Spanish AECC (M.L.M.-C.). Mice studies were supported in part by Abbott Laboratories GmbH (Hannover, Germany).

Supplementary Materials and Methods

Metabolomics Analyses: Serum and Liver Samples

Targeted serum metabolic profiles were semiquantified as previously described.[1] Briefly, ultra-high performance liquid chromatography–single-quadrupole–MS amino acid analysis system was combined with 2 separate ultra-high performance liquid chromatography–time of flight–MS–based platforms analyzing methanol and chloroform/methanol serum extracts. Identified ion features in the methanol extract platform included fatty acids, oxidized fatty acids, acyl carnitines, N-acyl ethanolamines, bile acids, steroids, and lyso-phospholipids. The chloroform/methanol extract platform covered glycerolipids, cholesteryl esters, sphingolipids, diacyl-phospholipids, acyl-ether-phospholipids, and primary fatty acid amides. Lipid nomenclature and classification follows the LIPID MAPS convention (www.lipidmaps.org).

Liver metabolic profiles were analyzed as described.[1,2] The previous 3 ultra-high performance liquid chromatography–MS platforms mentioned in serum analysis were completed with a methanol/water extract platform.[2] This platform covered polar metabolites, such as vitamins, nucleosides, nucleotides, carboxylic acids, coenzyme-A derivatives, carbohydrate precursors/derivatives, and redox-electron-carriers.

Metabolomics data were preprocessed using the TargetLynx application manager for MassLynx 4.1 (Waters Corp, Milford, MA). Intrabatch normalization followed the procedure described.[3]

One Central Carbon Metabolism Measurement in Liver Samples

Extraction of the main metabolites belonging to the methionine pathway were performed as described.[4] Briefly, livers (50 mg) were disrupted and metabolite was extracted in ice-cold methanol/water (50/50 %vol/vol) containing 10 mmol/L acetic acid in a tissue homogenizer (Precellys, Montigny-le-Bretonneux, France) in 2 × 20" cycles at 6000 rpm. After centrifugation and evaporation, pellets were resuspended in water/MeCN/formic acid (40/60/0.1 %vol/vol/vol) for injection on the ultra-high-performance liquid chromatography–MS system. For the analysis of serum samples, 40-μL aliquots of serum were diluted with 40 μL water containing 0.2% formic acid (%vol/vol) and proteins were precipitated by addition of 120 μL of acetonitrile. Samples were sonicated for 10 minutes at 4°C and centrifuged at 14,000 rpm for 30 minutes at 4°C. The supernatant was injected directly onto the ultra-high-performance liquid chromatography–MS system.

Samples were analyzed with an ultra-high-performance liquid chromatography system (Acquity; Waters, Manchester, UK) coupled to a time-of-flight–mass spectrometer (SYNAPT G2; Waters). A 2.1 × 100 mm, 1.7-μm BEH amide column (Waters), thermostated at 40°C, was used to separate the analytes before entering the MS. Solvent A (aqueous phase) consisted of 99.5% water, 0.5% formic acid, and 20 mmol/L ammonium formate, whereas solvent B (organic phase) consisted of 29.5% water, 70% MeCN, 0.5% formic acid, and 1 mmol/L ammonium formate.

To obtain a good separation of the analytes the following gradient was used: from 5% A to 50% A in 2.4 minutes in curved gradient (#8, as defined by Waters), from 50% A to 99.9% A in 0.2 minutes constant at 99.9% A for 1.2 minutes, back to 5% A in 0.2 minutes. The flow rate was 0.250 mL/min and the injection volume was 2 μL. All samples were injected randomly. After every 8 injections a high and a low quality control sample was injected. If necessary, signals were corrected for signal drift during the run. All samples were injected in duplicate.

The MS was operated in positive electrospray ionization mode in full scan (50–1200 daltons) with a capillary voltage of 250 V, a sampling cone voltage of 20 V, and an extraction cone voltage of 5 V. Source and desolvation temperatures were 120°C and 450°C, respectively. Cone and desolvation gas flows were 5 and 600 L/h, respectively. The MS was tuned to a mass resolution of 20,000 full width at half maximum. Scan time was 0.2 seconds. A lock mass was used to correct for instrument fluctuations during the run. Therefore, leucine–enkephalin (2 μg/mL) was infused at 10 μL/min and its signal was measured every 40 seconds for 0.2 seconds.

Extracted ion traces were obtained for methionine (m/z, 150.0589), SAMe (m/z, 399.1451), S-adenosylhomocysteine (m/z, 385.1294), methylthioadenosine (m/z, 298.097), decarboxylated SAMe (m/z, 355.1552), spermine (m/z, 203.2236), spermidine (m/z, 146.1657), GSH (m/z, 308.0916), and choline (m/z, 104.1070) in a 20 millidalton window and subsequently smoothed (2 points, 2 iterations) and integrated with QuanLynx software (Waters). Peak areas were obtained from the extracted ion chromatograms and normalized to milligram of tissue or milliliter of serum.

Quantification of Total Lipids

Livers (300 mg) were homogenized and lipids were extracted as described.[5] TGs were quantified using a kit (A. Menarini Diagnostics, Florence, Italy). PE, PC, and DG were separated by thin-layer chromatography and quantified as described.[6]

Nucleic Acid Isolation and Quality Controls

Total DNA was extracted from mouse liver tissue with the AllPrep DNA/RNA Mini Kit (Qiagen, Hilden, Germany), following the recommended procedures. The concentration of DNA was measured using Qubit (Life Technologies, Waltham, MA), and its integrity was checked by agarose gels in case of DNA.

Global DNA Methylation Profiles

Global DNA methylation was analyzed by reduced representation bisulfite sequencing (RRBS). Sequencing

libraries were prepared with a modification of the method described by Varela-Rey et al,[7] digesting DNA with *Taq*I and *Msp*I and using the NEXTflex Bisulfite-Seq Kit, Illumina Compatible (Bioo Scientific, Austin, TX), and Single-Read sequenced on a HiScanSQ platform (Illumina Inc, San Diego, CA) for 50 nucleotides. Resulting multiplexed FASTQ files for each sample were merged into a single FASTQ before the quality control and filtering steps. Quality control and adapter trimming were performed via FASTQC (http://www.bioinformatics.babraham.ac.uk/projects/fastqc/) and Trim Galore (http://www.bioinformatics.babraham.ac.uk/projects/trim_galore/), and only those with a minimum of 20 phred quality score were retained. Bisulfite reads were mapped to mm10 (*Mus musculus*) reference genome. Reads were mapped using Bismark, which is developed specifically to map bisulfate-treated reads.[8] In this analysis, 2 alignment mismatches (n = 2) were allowed. Resulting alignment files, in SAM format, were sorted before being used as input for the methylKit (R-package) to call DMRs, compute methylation ratios, and perform a DMR analysis.[9]

Determination of Hepatocyte Mitochondrial Membrane Potential

Hepatocytes were isolated from wild-type and MAT1A-KO mice and incubated with 4 mmol/L SAMe for 4 hours. The JC-1 dye (Mitochondrial Membrane Potential Probe; Life Technologies) was used to evaluate mitochondrial membrane potential according to the manufacturer's instructions. Briefly, cells were incubated in 1.5 mL culture medium containing 10 μg/mL JC-1 for 10 minutes at 37°C in a 5% CO_2 atmosphere. The cells then were washed twice with cold phosphate-buffered saline, trypsinized, suspended in 1 mL phosphate-buffered saline/1% fetal bovine serum, and immediately analyzed by flow cytometry using an LSRII flow cytometer (BD Biosciences, San Agustin de Guadalix, Madrid, Spain) and Flowjo software (FlowJo, Ashlan, OR) . The green fluorescence emission (JC-1 monomers) was monitored at 520 nm and the red-orange fluorescence emission (J-aggregates) was monitored at 590 nm. The aggregate/monomer ratio was calculated as a percentage of the maximal potential of wild-type hepatocytes (100%).

Western Blot

Frozen liver tissue samples were homogenized in lysis buffer (50 mmol/L Tris pH 8.5, 150 mmol/L NaCl, 5 mmol/L EDTA, 1% NP40, 1 mmol/L, complete protease inhibitor cocktail, and 50 mmol/L NaF) and centrifuged (10,000*g*, 20 minutes, 4°C). The protein concentration was determined by using the BCA Protein Assay Kit (Thermo Scientific, Waltham, MA). After quantification, 10–25 μg of protein were electrophoresed on sodium dodecyl sulfate–polyacrylamide gels and transferred onto membranes. Membranes were incubated with the next antibodies: diacylglycerol acyltransferase 2 (ab59493; Abcam, Cambridge, UK), stearoyl-CoA desaturase 1 (2794S; Cell Signaling Technology, Danvers, MA), and β-actin (A-5316; Sigma-Aldrich, St. Louis, MO). Band densities were analyzed by ImageJ (National Institutes of Health, Bethesda, MD) software. For densitometric quantification, levels of each protein for each sample were normalized to its loading control β-actin.

Histologic Staining

Sudan III staining. Ornithine carbamyl transferase–embedded frozen samples were sectioned, cleared with 60% isopropanol, and stained with Sudan III solution (0.5% in isopropanol Sudan III Panreac ref: 251731.1606) for 1 hour and finally cleared with 60% isopropanol. Sections were counterstained with Mayer hematoxylin (MHS32-1L; Sigma) and mounted in aqueous mounting medium for lipid quantification.

H&E and Sirius Red staining. Paraffin-embedded liver samples were sectioned, dewaxed with a Xylene substitute (HS-202, Histoclear; National Diagnostics, Atlanta, GA), and hydrated. Sections were stained for 5 minutes with Harry's hematoxylin (HHS128-4L; Sigma) and for 15 minutes with aqueous eosin (HT110232-1L; Sigma) for H&E staining or with 0.01% Fast green FCF in saturated picric acid for 15 minutes and 0.04% Fast green For Coloring Food/0.1% Sirius red in saturated picric acid for 15 minutes for Sirius red staining. Samples were dehydrated and cleared with Histoclear. Finally, sections were mounted in DPX mounting media (06522, 500 mL; Sigma).

In addition, liver sections were immunostained for detecting F4/80. F4/80 samples were unmasked with proteinase K during 15 minutes at room temperature. Endogenous peroxidase activity was blocked for 10 minutes with 3% hydrogen peroxide, then sections were blocked with 5% normal goat serum for 30 minutes and incubated with F4/80 (1:50, 1 hour at 37°C, MCA497BB; Bio-Rad, Hercules, CA) followed by 30 minutes with anti-Rat Immpress reagent (MP-7404; Vector, Burlingame, CA). Colorimetric detection was completed with Vector Vip purple substrate (sk-4600; Vector). Slides were counterstained with Mayer Hematoxylin (MHS32-1L; Sigma), and finally samples were dehydrated, cleared, and mounted in DPX mounting media (06522-500 mL; Sigma). Smooth muscle actin samples were counterstained with 4′,6-diamidino-2-phenylindole and mounted with Dako fluorescence mounting media (S3023; Dako, Carpinteria, CA).

For the analysis, 5 images per sample were taken with a 10× (H&E and Sirius Red), 20× (F4/80), or 40× (Sudan III) objective from an upright light microscope (Carl Zeiss AG, Oberkochen, Germany). Quantification of staining areas was performed using FRIDA software (http://bui3.win.ad.jhu.edu/frida/; Johns Hopkins University) and expressed as the percentage of stained area.

Proteomics

Frozen livers (n = 5) were ground while frozen in a liquid N_2 cooled cryohomogenizer (Retsch, Haan, Germany)

and then prepared for digestion. A total of 750 μg protein were denatured in a solution of 100 mmol/L TRIS-HCL, pH 8, and 8 mol/L urea. Samples then were ultrasonicated for 10 minutes in 10-second repeating on/off intervals of 10 seconds on and 10 seconds off (QSonica, Newtown, CT), and centrifuged at 16,000 $\times$ g for 10 minutes at 4°C to remove insoluble pellets. The soluble fraction then was reduced with dithiothreitol (15 mM) for 1 hour at room temperature and alkylated with iodoacetamide (15 mmol/L) for 30 minutes at room temperature in the dark. Then, 75 μg protein was diluted to a final concentration of 2 mol/L urea with 100 mmol/L TRIS-HCL, pH 8, and digested overnight on a shaker at 37°C in 3 μg of trypsin/Lys-C mix (Promega, Madison, WI). Samples were de-salted and cleaned using HLB plates (Oasis HLB 30 μm, 5 mg sorbent; Waters).

LC-MS/MS was performed on a Dionex Ultimate 3000 NanoLC connected to an Orbitrap Elite (Thermo Fisher) equipped with an EasySpray ion source. The mobile phase A comprised 0.1% aqueous formic acid and mobile phase B comprised 0.1% formic acid in acetonitrile. Peptides were loaded onto the analytical column (PepMap RSLC C18 2 μm, 100 Å, 50 μm i.d. $\times$ 15 cm) at a flow rate of 300 nL/min using a linear AB gradient composed of 2%–25% A for 185 minutes, 25%–90% B for 5 minutes, then an isocratic hold at 90% for 5 minutes with re-equilibrating at 2% A for 10 minutes. The temperature was set to 40°C for both columns. Nano-source capillary temperature was set to 275°C and spray voltage was set to 2 kV. MS1 scans were acquired in the Orbitrap Elite at a resolution of 60,000 full width at half maximum with an automated gain control target of 1 $\times$ 106 ions over a maximum of 500 ms. MS2 spectra were acquired for the top 15 ions from each MS1 scan in normal scan mode in the ion trap with a target setting of 1 $\times$ 104 ions, an accumulation time of 100 ms, and an isolation width of 2 daltons. Normalized collision energy was set to 35% and 1 microscan was acquired for each spectra.

For preparative data analysis and peptide identification search, the raw MS files were converted to mzXML using MSConvert and searched against the Swiss-Prot–reviewed mouse FASTA database (33,330 proteins and decoys) using the COMET, X! Tandem native, and X! Tandem k-score search algorithms.[10,11] Target-decoy modeling of peptide spectral matches was performed with peptide prophet[12] and peptides with a probability score of >95% from the entire experimental data set were imported into Skyline software[13] to establish a library for quantification of precursor extracted ion intensities. Precursor extracted ion intensities from each experimental file were extracted against the Skyline library, and peptide extracted ion intensities with isotope dot product scores greater than 0.8 and a minimum of 2 peptides per protein were filtered for final statistical analysis of proteomic differences.[14] Normalization of raw peptide intensities and protein level abundance inference were calculated using the linear mixed-effects model built into the open sources MSSTATs (v3.2.2) software suite.[15]

References

1. Barr J, Caballeria J, Martinez-Arranz I, et al. Obesity-dependent metabolic signatures associated with nonalcoholic fatty liver disease progression. J Proteome Res 2012;11:2521–2532.
2. Martínez-Uña M, Varela-Rey M, Cano A, et al. Excess S-adenosylmethionine reroutes phosphatidylethanolamine towards phosphatidylcholine and triglyceride synthesis. Hepatology 2013;58:1296–1305.
3. Martinez-Arranz I, Mayo R, Pérez-Cormenzana M, et al. Enhancing metabolomics research through data mining. J Proteomics 2015;127:275–288.
4. van Liempd S, Cabrera D, Mato JM, et al. A fast method for the quantitation of key metabolites of the methionine pathway in liver tissue by high-resolution mass spectrometry and hydrophilic interaction ultra-performance liquid chromatography. Anal Bioanal Chem 2013; 405:5301–5310.
5. Bligh EG, Dyer WJ. A rapid method of total lipid extraction and purification. Can J Biochem Physiol 1959; 37:911–917.
6. Ruiz JI, Ochoa B. Quantification in the subnanomolar range of phospholipids and neutral lipids by monodimensional thin-layer chromatography and image analysis. J Lipid Res 1997;38:1482–1489.
7. Varela-Rey M, Iruarrizaga-Lejarreta M, Lozano JJ, et al. S-adenosylmethionine levels regulate the Schwann cell DNA methylome. Neuron 2014;81:1024–1039.
8. Krueger F, Andrews SR. Bismark: a flexible aligner and methylation caller for Bisulfite-Seq applications. Bioinformatics 2011;27:1571–1572.
9. Akalin A, Kormaksson M, Li S, et al. Methyl Kit: a comprehensive R package for the analysis of genome-wide DNA methylation profiles. Genome Biol 2012; 13:R87.
10. Eng JK, Jahan TA, Hoopmann MR, et al. Comet: an open-source MS/MS sequence database search tool. Proteomics 2013;13:22–24.
11. Craig R, Beavis RC. TANDEM: matching proteins with mass spectra. Bioinformatics 2004;20:1466–1467.
12. Keller A, Nesvizhskii AI, Kolker E, et al. Empirical statistical model to estimate the accuracy of peptide identifications made by MS/MS and database search. Anal Chem 2002;74:5383–5392.
13. MacLean B, Tomazela DM, Shulman N, et al. Skyline: an open source document editor for creating and analyzing targeted proteomics experiments. Bioinformatics 2010; 26:966–968.
14. Schilling B, Rardin MJ, MacLean BX, et al. Platform-independent and label-free quantitation of proteomic data using MS1 extracted ion chromatograms in skyline: application to protein acetylation and phosphorylation. Mol Cell Proteomics 2012;11:202–214.
15. Choi M, Chang CY, Clough T, et al. MSstats: an R package for statistical analysis of quantitative mass spectrometry-based proteomic experiments. Bioinformatics 2014;30:2524–2526.

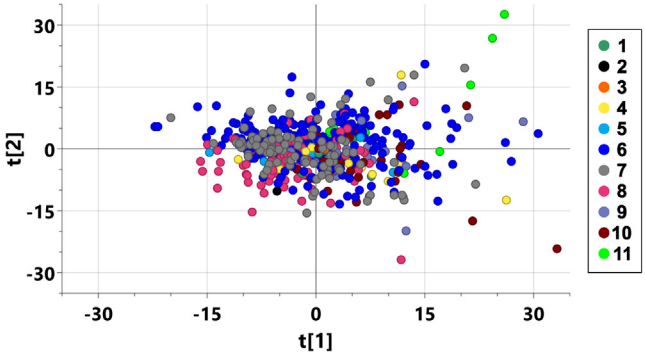

Supplementary Figure 1. PCA of 535 samples from the 11 participating hospitals. PCA analysis showed that patients (N = 535) clustered together independently of the hospital of origin. Each *dot* represents 1 sample and each color represents a different hospital: (1) Hospital Universitario "12 de Octubre", Madrid, Spain; (2) Hospital Clínic, Barcelona, Spain; (3) Hospital del Tajo, Aranjuez, Spain; (4) Hospital General Universitario Gregorio Marañón, Madrid, Spain; (5) Pitié-Salpêtriere Hospital, Paris, France; (6) Hospital Universitario Marques de Valdecilla, Santander, Spain; (7) Hospital Universitario Príncipe de Asturias, Madrid, Spain; (8) Hospital Universitario Reina Sofía, Córdoba, Spain; (9) Hospital Universitario Santa Cristina, Madrid, Spain; (10) Hospital Nuestra Señora de Valme and Hospital Universitario Virgen Macarena y Virgen del Rocío, Sevilla, Spain; and (11) Hospital Clínico Virgen de la Victoria, Malaga, Spain.

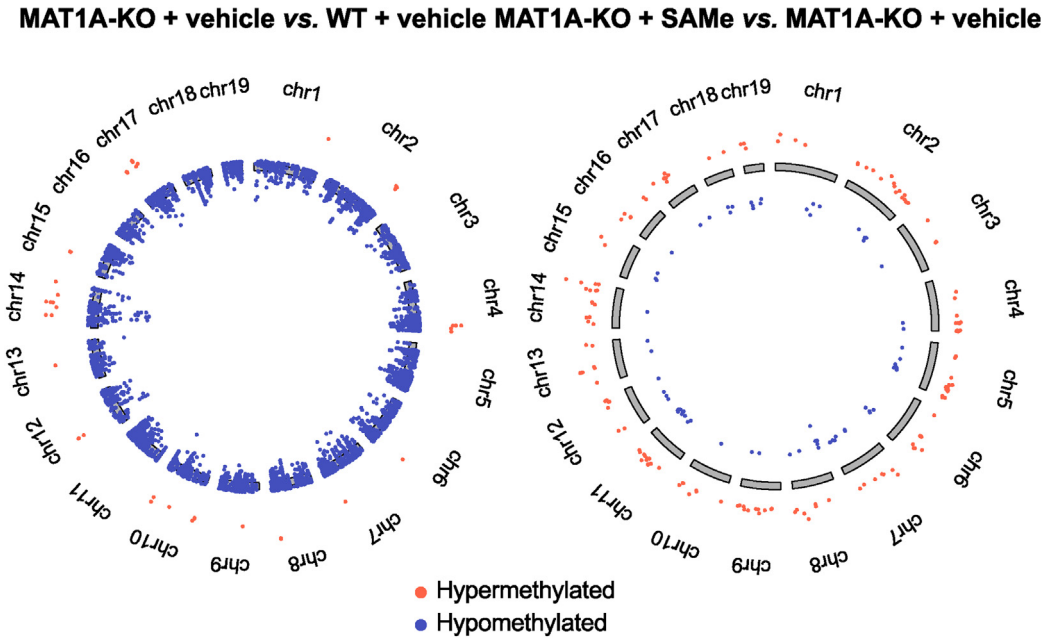

DMR*	MAT1A-KO + vehicle *vs.* WT + vehicle	MAT1A-KO + SAMe *vs.* WT + vehicle	MAT1A-KO + SAMe *vs.* MAT1A-KO + vehicle
Hypermethylated	43	53	161
Hypomethylated	6678	5330	69
Total	6721	5383	230

*Filtering parameters: *Q*-value < .05, methylation difference > 20%

Supplementary Figure 2. Effect of SAMe treatment on global DNA methylation and NASH progression in MAT1A-KO mice. Circos plots of the DMRs between MAT1A-KO + vehicle and WT + vehicle (*left*) and MAT1A-KO+SAMe and MAT1A-KO + vehicle (*right*). *Red spots* and *blue spots* represent hypermethylated and hypomethylated regions, respectively. The table shows the number of hypermethylated, hypomethylated, and total DMRs in each comparative performed (MAT1A-KO + vehicle vs WT + vehicle; MAT1A-KO + SAMe vs WT + vehicle, and MAT1A-KO + SAMe vs MAT1A-KO + vehicle).

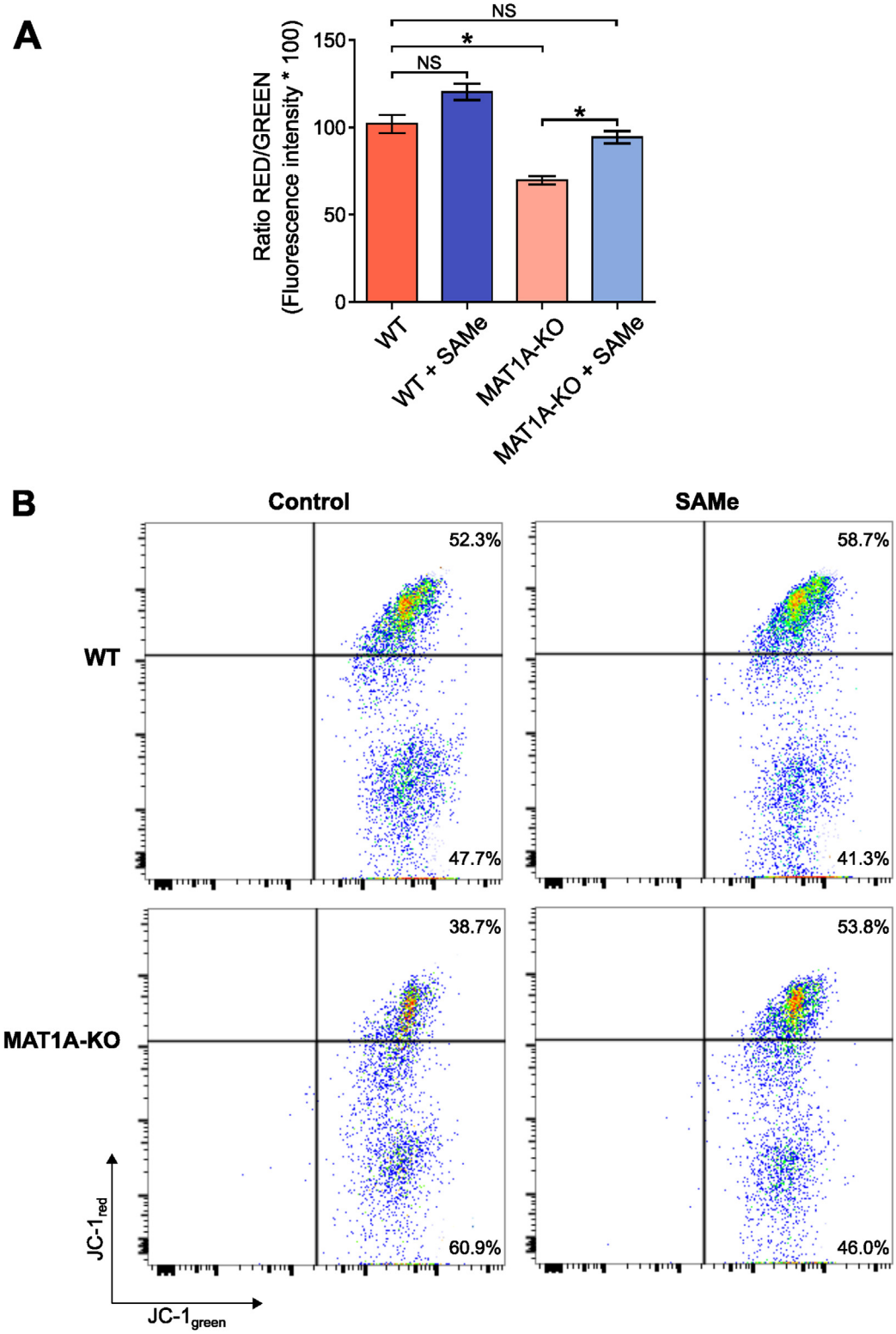

Supplementary Figure 3. Mitochondrial membrane polarization was restored in MAT1A-KO mice upon incubation with SAMe. (*A*) WT and MAT1A-KO hepatocytes were incubated for 4 hours with 4 mmol/L SAMe or vehicle. The cells then were stained with 10 μg/mL of the dye JC-1, and assessed for red and green fluorescence by flow cytometry. The data represent the variation of the ratio between red and green fluorescence intensity relative to WT control hepatocytes (100%) performed in triplicate and are representative of 2 independent experiments. *Student *t* test, $P < .05$. (*B*) Representative flow cytometric analysis of WT and MAT1A-KO hepatocytes treated with SAMe or vehicle. The percentage of JC-1_{red}^{high}/JC-1_{green}^{high} and JC-1_{red}^{low}/JC-1_{green}^{high} populations is presented. The data are representative of 2 independent experiments performed in triplicate.

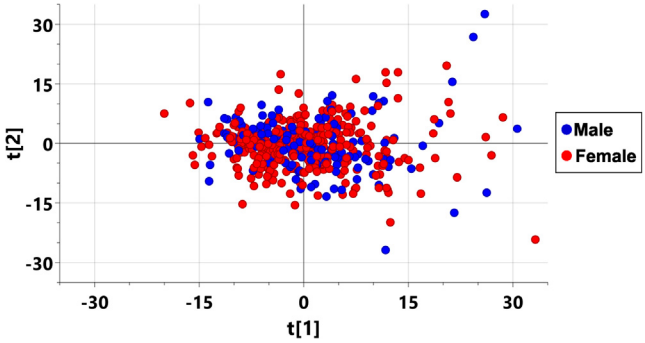

Supplementary Figure 4. PCA plot of human serum samples classified according to sex. PCA analysis showed that males (30%) and females (70%) clustered together. Each individual is represented by 1 *dot* and the color corresponds to females (red) and males (blue).